Int. J. Electrochem. Sci., 14 **(2019)** 1040 – 1068, doi: 10.20964/2019.01.83

International Journal of
ELECTROCHEMICAL
SCIENCE
www.electrochemsci.org

Synthesis of Polymers Containing Residues of Biogenic Amino Acid Methionine, Methionine Sulfoxide and Methionine Sulfone and Their Application as Inhibitors of Mild Steel Corrosion

Mohammad Abu Jafar Mazumder

Chemistry Department, King Fahd University of Petroleum and Minerals, Dhahran 31261, Saudi Arabia
E-mail: jafar@kfupm.edu.sa

Received: 25 November 2017 / *Accepted:* 2 November 2018 / *Published:* 30 November 2018

Ethyl ester hydrochloride of L-methionine **I** was converted to its *N*,*N*-diallyl derivative **II** which upon treatment with HCl led to *N*,*N*-diallyl methionine ethyl ester hydrochloride **III**. Cationic monomer **III** underwent cyclopolymerization to give polymer sulfide **IV,** embedded with five-membered pyrrolidine rings, which upon oxidation in the presence of 1 and 2 equivalents of H_2O_2 afforded polymer sulfoxide **V** and polymer sulfone **VI**, respectively. The thermal stability, intrinsic viscosity and critical micelle concentrations of these polymers were determined. The inhibition efficiency obtained from gravimetric weight loss, were corroborated by the findings of potentiodynamic polarization and electrochemical impedance spectroscopy. The critical micelle concentration of the polymers **IV-VI** has been determined to be ≈6 ppm. At a concentration of ≈ 5.5 ppm in 1.0 M HCl, the polymers **IV-VI** imparted remarkable corrosion inhibition efficiency (IE) of 86, 87 and 83%, respectively; while in the presence of 22.8 ppm of polymer sulfoxide **V**, an IE of 97% was achieved. The potentiodynamic polarization and EIS studies suggested that the polymer chains form a protective layer and quarantine the metal surface from the corrosive environment. The XPS and SEM-EDX supported the adsorption and the film forming ability of the studied polymer compounds on the metal surface.

Keywords: Cyclopolymerization; Methionine sulfide; Methionine sulfoxide; Methionine sulfone; Mild steel; Corrosion inhibition.

1. INTRODUCTION

Mild steel having low carbon content (upto 0.3%) is readily available, cheap and found huge applications in oil and gas industries due to its notably high mechanical properties [1]. Despite its immense properties and applications, mild steel is highly susceptible to corrosion. The rusting and

scale formation is a worldwide problem in different oil and gas industries in transmission pipelines [2]. In most cases, hydrochloric acid and/or sulfuric acid have been used to remove these rusts, scales and sludges. The other important industrial applications of acid are oil-well acid in oil recovery, industrial acid cleaning, acid pickling, acid descaling and etching of metal alloys [3,4]. The mild steel becomes very vulnerable with continuous use of acids in various industrial processes [5]. The use of inhibitors is one of the most practical methods to protect mild steel from corrosion particularly in acid media.

Different types of organic and inorganic compounds are widely explored as corrosion inhibitors for the protection of metal surfaces to eliminate or reduce corrosion inhibition [6]. Inhibition of metal corrosion by synthetic inhibitors is influenced by the presence of heteroatoms whose efficacies are known to increase in the order of O < N < S < P [7]. Noted that nitrogen-containing heterocyclic molecules are found to be effective corrosion inhibitors [8]. The inhibitor molecules usually interfere with anodic or cathodic reactions occurring on the metal surfaces to minimize or eliminate corrosion processes [9]. However, most of the synthetic inhibitors were found to be not only expensive, but also toxic and cause health problems [10]. Therefore, it is an utmost demand in these days to replace the synthetic inhibitors by a cheap, non-toxic, most effective and environment friendly corrosion inhibitors.

Amino acids are biocompatible and biodegradable naturally occurring compounds which have been used in pharmaceuticals and biological applications for many decades [11,12]. Amino acids have also been reported as effective corrosion inhibitors in different aggressive media [2,13,14]. Alanine and glycine were explored for inhibition of mild steel corrosion in 0.1 M HCl and found to impart inhibition efficiency (IE) of 80 and 78.9%, respectively at 10 mM [15]. The alanine, cysteine and *S*-methyl cysteine amino acids have been studied as potential corrosion inhibitors for iron in 1.0 M HCl, and the maximum inhibition efficiencies were reported to be 77.3, 86.0 and 94.2%, respectively, at 5.0 mM [8]. The non-toxic and readily available methionine at 25 ppm has also been explored for mild steel corrosion in 0.1 M HCl, and the IE was reported to be 47% [16]. Methionine (149 ppm), methionine sulfoxide (165 ppm) and methionine sulfone (181 ppm) were studied in 1.0 M HNO_3 for copper corrosion, and were reported to impart IE of 79, 85 and 88%, respectively [17]. Cationic, anionic and non-ionic surfactants as well as halide ions have been added to the amino acid L-cysteine for the improvement of inhibition efficiency of amino acid, but no significant improvement of IE was observed [18].

In recent years, polymers received particular attention as corrosion inhibitors [19,20]. Polymers are relatively cheap, stable, have large surface area, and possess multiple anchoring sites as a form of atoms and/or functional groups which help forming a bond with metal ions and/or adsorption onto the metal surface. As the polymer-metal complex can block the metal surface, the active sites of the metal surface are thus protected from the corrosive environment [21]. Polyvinylpyrrolidone and polyethylenimine in H_3PO_4 have been used to study the corrosion IE for low carbon steel. The polymers were found to be mixed inhibitors predominantly inhibiting the anodic corrosion reactions [22].

In this article, we report the synthesis of a group of cyclopolymers having skeleton of pyrrolidine ring embedded in the polymer chains (Scheme 1). The immensely important Butler's cyclopolymerization protocol [23-25], used in the synthesis, led to polymers **4**, **5** and **6**, the repeating

unit of which contained the residues of amino acid methionine, methionine sulfoxide and methionine sulfone, respectively. The presence of pH-responsive N along with O and S as well as multiple anchoring points in a polymer chain has provided us an opportunity to examine and compare the efficacy of the functional motifs of the sulfide, sulfoxide and sulfone in the inhibition of mild steel corrosion in 1.0 M HCl. The corrosion efficiency and adsorption characteristics of these potentially green polymers on mild steel has been evaluated by gravimetric and various electrochemical techniques as well as X-ray photoelectron spectroscopy (XPS), and scanning electron microscopy (SEM) and energy dispersive X-ray spectroscopy (EDX).

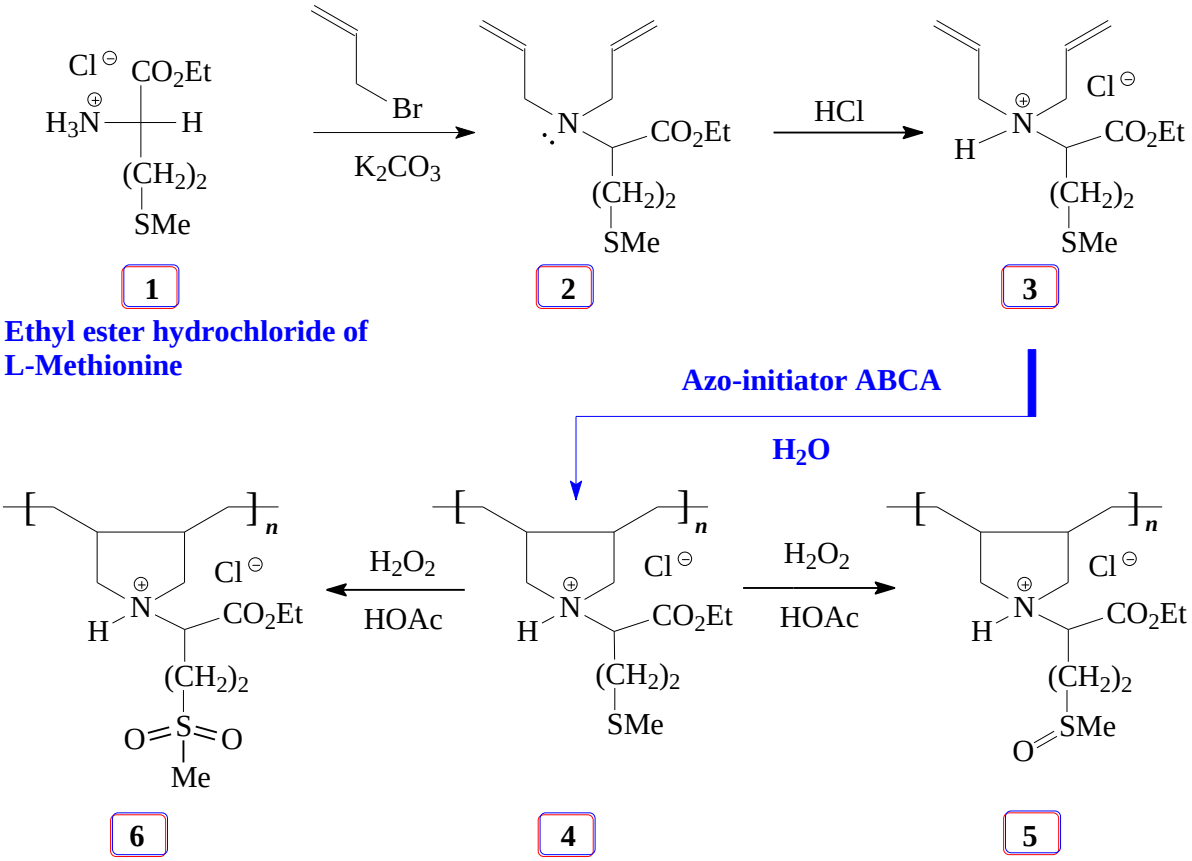

Scheme 1. Synthesis of methionine-based polymers containing sulfide **4**, sulfoxide **5**, and sulfone **6** motifs.

2. EXPERIMENTAL

2.1. Materials and test solution

Ethyl ester hydrochloride of L-Methionine **1** was obtained from Fluka Chemie AG. Hydrogen peroxide (35% w/v), hydrochloric acid (37% w/v), acetic acid and potassium carbonate (K_2CO_3) were purchased from BDH Chemical Ltd (Pool, England), and used as received. Allyl bromide and 4,4′-

azobis(4-cyanovaleric acid) (ABCA) (Fluka Chemie AG) were used as received. All solvents were of HPLC grade. Water was purified and de-ionized using a Milli-Q system from Millipore. All glassware was cleaned using de-ionized water. Diallyl derivative of methionine **2** was prepared from L-methionine ethyl ester hydrochloride **1** as described [26]. HCl solution was prepared from concentrated HCl (37%, reagent grade) by diluting to 1.0 M with distilled de-ionized water. The corrosion inhibitors were dissolved in 1.0 M HCl solution at required concentrations in µM, and 1.0 M HCl solution in the absence of inhibitor was taken as blank.

2.2. Characterization

Perkin Elmer 16F PC FTIR was used to record IR spectra, while ^{1}H and ^{13}C NMR were collected in a Nuclear Magnetic Resonance (JEOL LA 500 MHz) spectrometer. Elemental analysis was performed by an elemental analyzer (Perkin Elmer; Carlo-Erba: 2400). The viscosity values of synthesized compounds were determined in CO_2-free water using an Ubbelohde viscometer (Viscometer Constant 0.005317 mm^2 s^{-2}). Thermogravimetric analysis (TGA) was performed using Platinum/Platinum–Rhodium (Type R) thermocouples under N_2 (flow rate 50 mL/min) using an SDT thermogravimetric analyzer (Q600: TA Instruments, New Castle, DE, USA) by stepping up the temperature (10 °C/min) over 20–800 °C. A potentiostat-galvanostat (Autolab, Booster 10A-BST707A) connected with a computer was used for the electrochemical measurements. Surface tension was measured using a surface tensiometer (PHYWE, Germany) equipped with a torsion dynamometer (0.01 N) and platinum iridium ring having a diameter of 1.88 cm.

2.3. Synthesis

2.3.1. General procedure for the preparation of polymer sulfide (4)

The polymer sulfide **4** was prepared following the Butler's cyclopolymerization protocol [25, 26]. The monomer precursor **2** (5.72 g; 18.6 mmol), and 4,4′-azobis(4-cyanovaleric acid) (ABCA) (0.963 g, 3.44 mmol, 16 mol% relative to monomer) were dissolved in de-ionized water (0.670 g) and conc. HCl (37% ; 2.39 g, 24.3 mmol) in a 25 mL round bottom flask. The solution was gently bubbled with nitrogen for 5 min, then heated the flask at 85 °C for 36 h. After the elapsed time, the crude polymer was dissolved in de-ionized water (8 mL) and conc. HCl (37%) (3 mL), dialyzed against de-ionized water in cellulose tubing (6-8 kDa MW cutoff, spectrum laboratories) for 24 h. The milky polymer solution was then freeze dried to give polymer **4.** Yield: 4.87 g (85%). Elemental analysis of $C_{13}H_{24}ClNO_2S$: Calculated: C, 53.14; H, 8.23; N, 4.77; S, 10.91; found: C, 53.56; H, 9.16; N, 5.40; S, 11.01. $\nu_{max.}$ (KBr) 3441, 2984, 2927, 2854,1742, 1635, 1445,1372, 1208, 1160, 1100, 1021, and 853 cm^{-1}. The thermal decomposition of polymer sulfide **4**: 250-270 °C (decomposed, turned black).

2.3.2. Conversion of polymer sulfide (4) to polymer sulfoxide (5)

Polymer **4** (0.844 g; 2.74 mmol) was dissolved in glacial acetic acid (2.50 g) in a 10-mL round bottom flask. Hydrogen peroxide (297 mg, 35% w/v; 3.06 mmol) was then slowly added to the

reaction mixture, and stirred at room temperature until the ^{1}H NMR indicated that the sulfide completely converted to sulfoxide **5**. After the elapsed time, the crude polymer solution was poured into a dialysis membrane (6-8 kDa MW cutoff, spectrum laboratories), and dialyzed against de-ionized water for 8 h. The resultant polymer **5** was then freeze-dried. Yield: 0.807 g (91%). Elemental analysis of $C_{13}H_{24}ClNO_3S$: Calculated: C, 50.39; H, 7.81; N, 4.52; S, 10.35%; Found: C, 50.4; H, 7.7; N, 4.5; S, 10.2; ν_{max} (KBr) 3396, 2936, 2608 (br), 2361, 1741, 1633, 1451, 1379, 1298, 1212, 1130, 1014, 948, and 853 cm^{-1}. The thermal decomposition of polymer sulfoxide **5**: 240-260 °C (decomposed, turned black).

2.3.3. Conversion of polymer sulfide (4) to polymer sulfone (6)

Polymer **4** (2.11 g; 6.86 mmol) was dissolved in glacial acetic acid (6.25 g) in a 10-mL round bottom flask, hydrogen peroxide (2.35 g, 35% w/v; 24.2 mmol) was then dropwise added to the reaction mixture. The reaction mixture was stirred at room temperature for 6 h. After the elapsed time, the crude polymer solution was dialyzed against de-ionized water for 4 h, followed by 1 h in 0.1 M HCl, and then additional 5 h in de-ionized water. Conc. HCl (37%) (0.6 mL) was added to the dialyzed polymer sample, and freeze-dried to obtain polymer sulfoxide **6**. Yield: 2.01 g (86%). Elemental analysis of $C_{13}H_{24}ClNO_4S$: Calculated C, 47.92; H, 7.42; N, 4.30; S, 9.84%; Found: C, 47.7; H, 7.3; N, 4.4; S, 9.9; ν_{max} (KBr) 3417, 2931, 2646 (br), 2361, 1742, 1638, 1451, 1380, 1299, 1214, 1131, 1019, 966, 850, 771, 770 and 669 cm^{-1}. The thermal decomposition of polymer sulfone **6**: 240-260 °C (decomposed, turned black).

2.4. Mild steel specimen

For gravimetric measurements, the rectangular shape mild steel coupon samples of size 2.5×2.0×0.1 cm^3 were used. For electrochemical polarization and impedance measurements, a flag shaped mild steel coupon (1 mm thick; exposure area: *ca.* 2 cm^2) with an approximate stem of 3 cm embedded by Araldite (RS, Saudi Arabia) were abraded by different grades of emery papers (grade 100 to 1500), rinsed with deionized distilled water, degreased with acetone followed by another wash by deionized distilled water and dried in a hot air at room temperature, and stored in a desiccator before use. The percent chemical composition of mild steel specimens used in gravimetric, electrochemical polarization and impedance measurements were as follow: C (0.089), Mn (0.34), Cr (0.037), Ni (0.022), Mo (0.007), Cu (0.005), V (0.005), P (0.010), Fe (99.47).

2.5. Corrosion tests

2.5.1. Gravimetric measurements

Gravimetric weight loss measurements were carried out in triplicate using pre-weighed mild steel coupons mentioned above were immersed in 250 mL of 1.0 M HCl solution in the absence or

presence of synthesized polymers for 6 h at 60 °C. After immersion time, the mild steel coupons were removed from the solution, washed with de-ionized water, dried to constant weight and re-weighed in order to determine the weight loss. The inhibition efficiency (η %) can be calculated from weight loss measurements using equation (1) :

$$\eta\ \% = \frac{W_b - W_i}{W_b} \times 100 \quad (1)$$

where W_b and W_i are the weight loss of the mild steel coupon in absence or presence of inhibitor (polymer), respectively.

2.5.2. Electrochemical measurements

A conventional three-electrode glass cell assembly consist of a mild steel specimen of *ca*. 2 cm^2 exposure area of a working electrode, saturated calomel electrode as a reference electrode and graphite (diameter: ≈ 5 mm) rod as a counter electrode. All the electrochemical tests were performed by a computer controlled Autolab potentiostat-galvanostat instrument (Model: 10A-BST707A, Netherlands), and NOVA (Version 1.8) software was used for processing and/or fitting and analyzing the electrochemical data. In all electrochemical experiments, the working electrode was immersed for 30 minutes to achieve the corrosion potential of mild steel.

Potentiodynamic polarization measurements were carried out at a sweep rate of 0.5 mV/s in the potential range from ± 250 mV with respect to the open circuit potential (OCP). The electrochemical parameters such as corrosion current density (i_{corr}), corrosion potential (E_{corr}), cathodic (β_c) and anodic (β_a) Tafel slopes were derived by extrapolation with respect to free corrosion potential from Tafel plots.

The inhibition efficiency (η %) values were calculated using the equation (2):

$$\eta(\%) = \left(\frac{i'_{corr} - i_{corr}}{i'_{corr}}\right)\ x\ 100 \quad (2)$$

where i_{corr} and i'_{corr} are the polarization resistances in absence or presence of polymer, respectively.

The linear polarization resistance (LPR) measurements were carried out to obtain polarization resistance (R_p) from current potential plots in the potential range from ±10 mV with respect to OCP. The inhibition efficiency (η %) and surface coverage (θ) were calculated using the following equations (3)- (4):

$$\eta(\%) = \left(\frac{R'_p - R_p}{R'_p}\right)\ x\ 100 \quad (3)$$

$$\theta = \left(\frac{C'_R - C_R}{C'_R}\right) \quad (4)$$

where R_p and R'_p are the polarization resistances in absence or presence of polymer, respectively. C_R and C'_R are the corrosion rate in absence or presence of polymer, respectively.

The electrochemical measurements were carried out in the frequency range 100 kHz to 50 mHz with a sinusoidal amplitude of 10 mV. The electrochemical impedance curves were plotted, and the electrochemical equivalent circuit parameters (R_p and CPE) and other parameters were obtained by fitting the Nyquist plot using NOVA (Version 1.8) software. The inhibition efficiency was then calculated using equation 3.

2.6. Surface analysis (XPS, SEM and EDX)

The XPS analysis was performed by an X-ray photoelectron spectrometer (Thermo Scientific, Model # Escalab 250 Xi). Avantage software was used to process the data. The C 1s peak at 285.4 eV was considered to be a reference peak. The XPS spectra were deconvoluted using a non-linear least squares algorithm with a Shirley base line and a Gaussian–Lorentzian combination.

The surface morphology of the corroded (blank) and inhibited (presence of polymer) metal surface was performed using a field-emission scanning electron microscope (FESEM, Lyra 3, Tescan, Czech Republic) with accelerating voltages of 20-30 kV. In addition, an energy dispersive X-ray (EDX) spectroscope (Oxford Inc., UK) fitted with an X-Max detector was used to determine the chemical compositions and mapping the levels of homogeneity of these metal surfaces. The SEM images were captured after immersing the steel samples at 60 °C for 6 h in absence (0 ppm) or presence of polymer (50 ppm).

3. RESULTS AND DISCUSSION

3.1. Synthesis of the polymers

Methionine ester hydrochloride **1** upon reacting with allyl bromide gave its diallyl derivative **2**, which was converted into monomer hydrochloride salt **3** (Scheme 1). At the outset, we were apprehensive about the polymerizability of cationic monomer **3** under free radical conditions since in addition to the presence of degradative chain transfer allylic motifs [27], the sulfide functionality can also act as a chain transfer agent. However, to our delight, monomer **3** in the aqueous solution readily underwent cyclocopolymerization in the presence of water-soluble free radical initiator ABCA to give polymer sulfide **4** in excellent yield. Polymer sulfide **4** upon oxidation in the presence of 1 and 4 equivalents of H_2O_2 at 20 °C afforded polymer sulfoxide **5** and polymer sulfone **6**, respectively, in excellent yields. The intrinsic viscosity [η] in 0.1 M HCl at 30 °C was determined using Mark Huggins viscosity relationship to be 0.0831, 0.0919 and 0.0846 dL g^{-1} for **4**, **5** and **6,** respectively. The aqueous solution behavior of polymer **4** having sulfide motifs was not normal; it gave a turbid mixture in water but soluble in 0.1 M HCl. On the other hand, the polymer sulfoxide **5** and polymer sulfone **6** were found to be water-soluble. The greater water-solubility of **5** and **6** could be attributed to the increasing polarity of the sulfoxide and sulfone motifs.

3.2. Polymer characterization (FT-IR, NMR and TGA)

The IR spectra of polymers **4**, **5**, and **6** were recorded by FT-IR (Perkin Elmer) in the frequency range 400-4000 cm^{-1}. The spectra revealed a strong absorption band at ≈1740 cm^{-1} attributed to C=O stretch of CO_2Et group. The strong bands at ≈ 1299 cm^{-1} and ≈1131 cm^{-1} are due to the sulfone motifs (O=S=O) stretching vibrations in **6**, while a band at ≈1019 cm^{-1} can be assigned to the S=O stretching absorption in **5**. The proton NMR spectra of polymer **4**, **5**, and **6** are presented in Fig. 1. The absence of alkene proton or carbon signals in the polymer spectra ascertains that the monomer has been converted to polymer. A closer look at the proton spectrum of **4**, **5** and **6** in D_2O showed the presence of CH_3 signals at 2.0, 2.6 and 3.0 ppm, respectively attributed to the presence of sulfide ($S\text{-}CH_3$) and sulfoxide [$S(=O)CH_3$] and sulfone [$S(=O)_2CH_3$] motifs. The ^{13}C signals around 170 ppm are attributed to the carbonyl groups in the repeating units of **4**, **5** and **6** (data not shown). The thermal degradation of the inhibitor molecules was examined by TGA to realize the chemical stability of the inhibitors. The TGA curves of polymers **4-6**, presented in Fig. 2, showed good thermal stability and no sudden weight loss has been observed up to 200 °C. Afterwards, the abrupt weight loss was observed which might be due to the thermal degradation of the polymers.

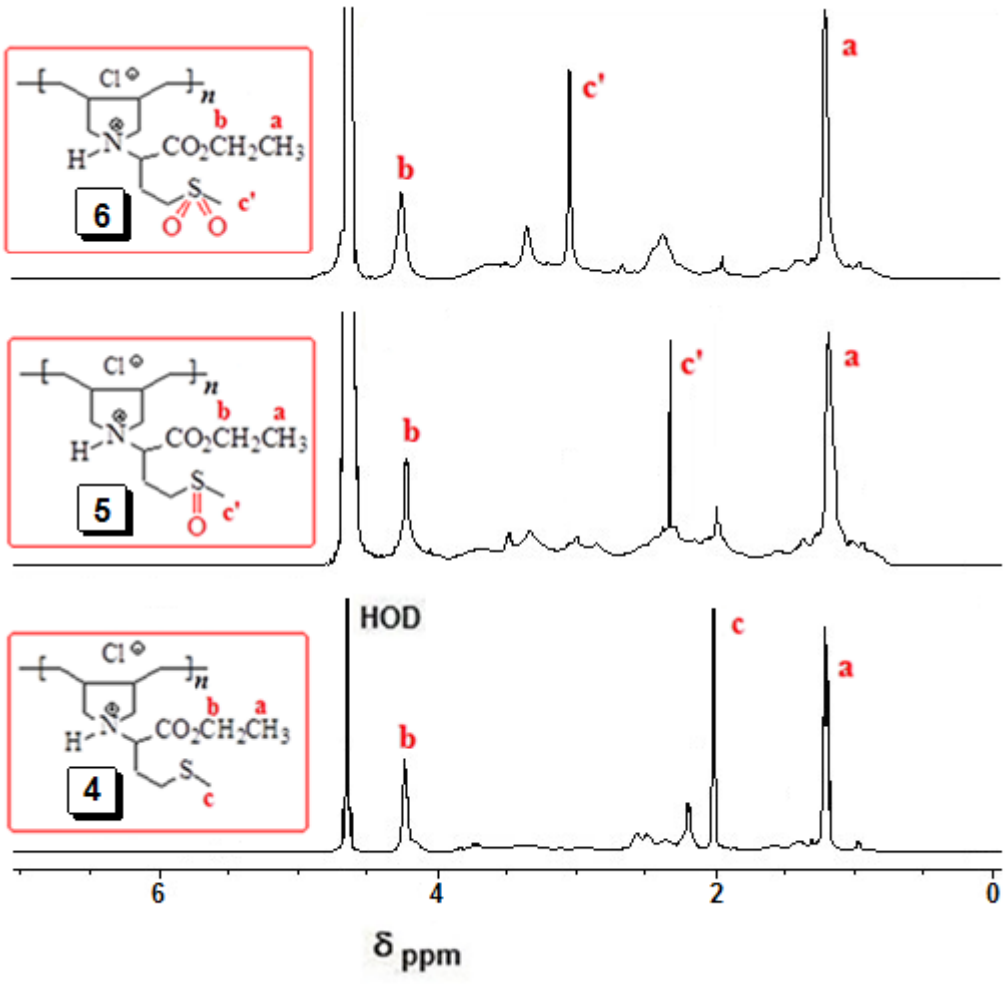

Figure 1. ^1H NMR spectra of (a) **4**, **(b) 5** and (c) **6** in D_2O.

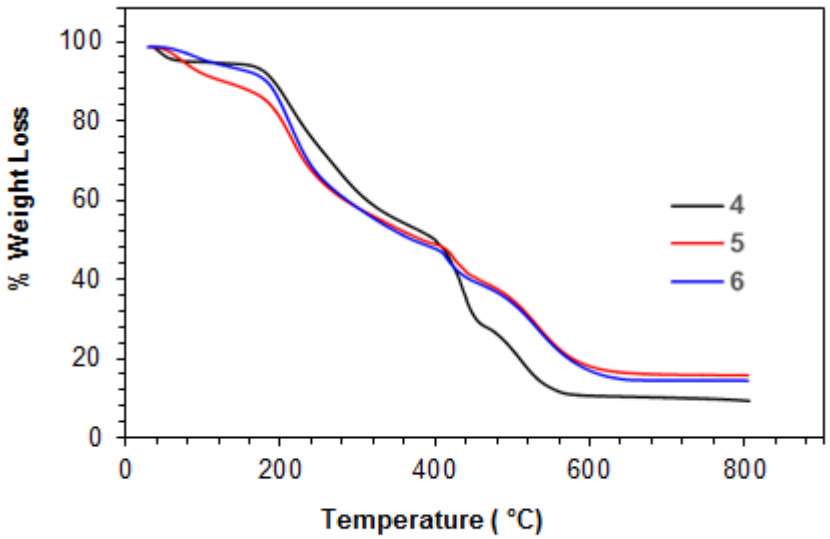

Figure 2. TGA curves of (a) **4**, **(b) 5** and (c) **6.**

3.3. Corrosion gravimetric measurements

The gravimetric weight loss data were collected after 6 h immersion of the mild steel coupons in the absence or presence of polymers **4**, **5**, and **6** in 1.0 M HCl at 60 ºC, and presented in Table 1. All the polymers demonstrated excellent IE in 1.0 M HCl at 60 ºC (Table 1). In the presence of 176 μM (i.e. ≈55 ppm) polymers **4**, **5**, and **6**, the η% were found to be 94.9, 97.7 and 89.4%, respectively, while at the polymer concentration of 35.2 μM (≈11 ppm), the corresponding η% values were calculated to be 93.7, 95.7 and 85.5%, respectively. It is apparent from the results that the IE increases with increasing the inhibitor concentrations, and reached a plateau indicating the completion of monolayer film on the metal surface. Polymer sulfoxide **5** provided the best protection; it imparted an IE of 96.1% at a concentration of 21.8 ppm (70.3 μM). Note that polymer sulfoxide **5**, at a meagre concentration of 1.5 ppm (4.84 μM) imparted a remarkable IE of 77%. The excellent IEs certifies the excellent inhibition efficacy of the functional motifs of sulfide, sulfoxide and sulfone for inhibiting the mild steel corrosion.

Table 1. The η% for different inhibitors for the inhibition of corrosion of mild steel exposed at 60 ºC in 1.0 M HCl for 6 h.

Compounds	Concentrations		Inhibition efficiency
	ppm (by wt.)	μM	η%)
1	15.0	70.3	45.2
	37.6	176	51.9
3	20.7	70.3	67.5
	51.7	176	73.4
4	0.54	1.75	56.4
	1.49	4.84	62.3

	2.70	8.78	76.1
	5.42	17.6	87.2
	8.07	26.2	92.8
	10.8	35.2	93.7
	21.6	70.3	94.3
	54.2	176	94.9
5	0.32	1.00	69.3
	0.57	1.75	77.0
	1.57	4.84	81.5
	2.84	8.78	84.9
	5.70	17.6	94.5
	8.48	26.2	95.7
	11.4	35.2	96.1
	22.8	70.3	97.7
	57.0	176	69.3
6	0.59	1.75	44.3
	1.64	4.84	58.5
	2.98	8.78	70.8
	5.98	17.6	83.4
	8.90	26.2	85.5
	11.9	35.2	85.9
	23.9	70.3	86.2
	59.8	176	89.4

While the high polarizability (softness) of sulfur in polymer sulfide **4** has a low affinity for hard acids like H^+ or Fe(III), it can act as a ligand for a less hard (softer) Fe(II) [28]. On the other hand, sulfoxides in polymer **5** are ambident ligands, which are capable of coordinating to metal ions *via* sulfur or oxygen (Scheme 2) [29,30]. In line with the hard-soft acid-base theory, sulfoxide complexes of Fe(II) (softer) and Fe(III) (harder) are reported to involve coordination *via* sulfur (softer) and oxygen (harder), respectively [31]. DMSO ($Me_2S=O$) coordinates to Fe(II) more strongly than does a sulfide compound (R_1R_2S). Significant stabilization for sulfoxide complex is understood to have resulted from a stronger iron to oxygen π back-bonding than the iron to sulfur π back-bonding [31].

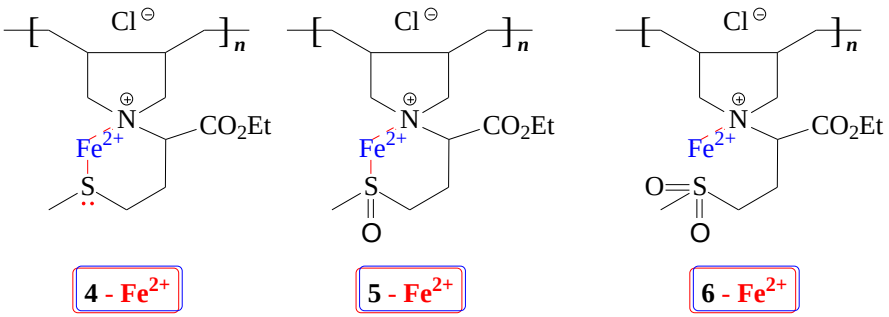

Scheme 2. Inhibitors protecting the anodic sites by a barrier film of metal-complexes.

The sulfur atom in sulfide **4**, sulfoxide **5** and sulfone **6** has two, one and zero lone pair of electrons, respectively. So, the absence of lone pair of electrons on sulfur in **6** preclude its participation in the coordination process leading to the decrease of the adsorption on metal surface as the process

mainly depends on the lone pairs on the oxygen atom [32]. The coordination ability on the iron surface is expected to follow the order: sulfoxide > sulfide > sulfone which is corroborated by the highest IEs for polymer sulfoxide 5 (Table 1).

3.4. Potentiodynamic polarization measurements

The required time to reach a stable OCP after immersing the mild steel coupon in 1.0 M HCl solution was determined in the absence (blank) or presence of different concentrations (1.75 and 176 µM) of synthesized inhibitors **4 - 6** at 60 °C. The variation of OCP and time curves are depicted in Fig. 3. For a blank solution, the OCP became stable very quickly with a value little bit less negative, corresponding to the free corrosion potential (E_{corr}) of the metal. However, in the presence of inhibitors, E_{corr} shifted more towards the positive direction and became stable after 20 min. The magnitude of the E_{corr} shifts increased with increase in the polymer concentration. The E_{corr} shift to the more noble direction is attributed to the preferential adsorption of the inhibitors on the anodic sites of the mild steel surface.

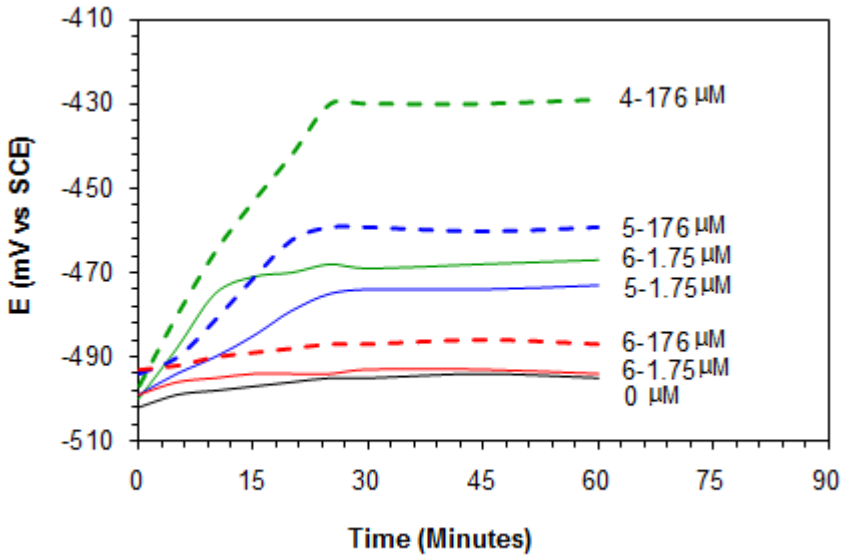

Figure 3. Variation of OCP of mild steel with time of immersion in 1.0 M HCl solution containing different concentrations (1.75 and 176 µM) of **4**, **5** and **6** at 60 ºC.

In addition to the gravimetric weight loss method, which is one of the simplest, convenient and consistent techniques (Table 1), the inhibition efficiencies of the synthesized inhibitors **4**, **5** and **6** were determined using different electrochemical methods (Tafel extrapolation, LPR and Impedance spectroscopy) for the corrosion of mild steel coupon after immersing in 1.0 M HCl solution at 60 ºC. The Tafel extrapolation and LPR results for inhibitors **4**, **5**, and **6** at different concentrations (1.75 to 176 µM) are tabulated in Tables 2 and 3, respectively. Some characteristics Tafel plots of polymers **4**-**6** in 1.0 M HCl solution are shown in Fig. 4. The η% by electrochemical methods (Tables 2 and 3) is corroborated by the findings of the gravimetric technique (Table 1). The inhibitive nature of the synthesized molecules was indicated by the significant decrease in the i_{corr} values. In the presence of

the inhibitor molecules **4** and **5** in 1.0 M HCl, the E_{corr} values of mild steel coupon have shifted to a positive direction, suggesting that the synthesized molecules perform as an anodic type of inhibitor, and mainly suppresses the anodic reaction. However, the relatively less change in the E_{corr} values were observed in presence of polymer compound **6** at a concentration ranges from 0-176 μM in 1.0 M HCl (Fig. 4). This could be attributed to lesser ability of sulfone group to form Fe(II)-complex at the anodic sites.

Table 2. Results of Tafel plots of a mild steel sample in 1.0 M HCl containing inhibitors **4, 5** and **6** at different temperature.

Sample	Temp (°C)	Concentrations		Tafel					
		ppm (by wt.)	μM	E_{corr} vs. SCE (mV)	β_a (mV dec^{-1})	β_c (mV dec^{-1})	I_{corr} (μA cm^{-2})	υ_{corr} (mm y^{-1})	η (%)[a]
4	60	0	0	–495	73.8	–169	2465	28.6	-
		0.54	1.75	–468	63.3	–110	1188	13.8	51.8
		1.49	4.84	–460	62.2	–108	922	10.7	62.6
		2.70	8.78	–457	63.7	–107	574	6.66	76.7
		5.42	17.6	–444	71.9	–104	355	4.12	85.6
		8.07	26.2	–442	84.4	–122	234	2.72	90.5
		10.8	35.2	–437	72.5	–86.2	197	2.29	92.0
		21.6	70.3	–436	97.7	–99.1	168	1.94	93.2
		54.2	176	–430	99.1	–102	160	1.86	93.5
5	50	0	0	–483	51.2	–117	505	5.85	-
		0.57	1.75	–479	68.1	–102	172	1.99	65.9
		1.57	4.84	–473	65.8	–117	145	1.68	71.2
		2.84	8.78	–460	72.3	–112	124	1.43	75.5
		5.70	17.6	–458	63.1	–128	99.5	1.15	80.3
		8.48	26.2	–455	64.3	–115	78.3	0.91	84.5
	60	0	0	–495	73.8	–169	2465	28.6	-
		0.32	1.00	–481	78.3	–119	870	10.1	64.7
		0.57	1.75	–475	62.2	–114	784	9.09	68.2
		1.57	4.84	–471	56.5	–105	584	6.78	76.3
		2.84	8.78	–470	55.8	–113	463	5.38	81.2
		5.70	17.6	–467	92.8	–157	335	3.89	86.4
		8.48	26.2	–466	88.9	–149	143	1.66	94.2
		11.4	35.2	–463	71.1	–103	106	1.23	95.7
		22.8	70.3	–461	72.4	–104	78.9	0.91	96.8
		57.0	176	–459	55.7	–117	61.6	0.72	97.5
	70	0	0	–498	60.9	–102	4508	52.3	-
		0.57	1.75	–489	69.0	–112	1790	20.8	60.3
		1.57	4.84	–487	58.2	–107	1474	17.1	67.3
		2.84	8.78	–486	53.5	–102	1240	14.4	72.5
		5.70	17.6	–478	56.4	–113	983	11.4	78.2
		8.48	26.2	–472	63.1	–105	807	9.36	82.1
6	60	0	0	–495	73.8	–169	2465	28.6	-
		0.59	1.75	–494	69.2	–104	1400	16.2	43.2
		1.64	4.84	–493	68.4	–113	1048	12.2	57.5
		2.98	8.78	–492	72.3	–112	749	8.69	69.6
		5.98	17.6	–492	76.1	–111	407	4.72	83.5

8.90	26.2	–490	85.5	–110	377	4.38	84.7
11.9	35.2	–488	81.6	–105	365	4.23	85.2
23.9	70.3	–488	70.1	–119	362	4.20	85.3
59.8	176	–487	76.8	–108	266	3.66	87.2

[a] Inhibition Efficiency, IE (i.e., η) = surface coverage θ.

Table 3. Results of LPR method in 1.0 M HCl containing inhibitors **4, 5** and **6** at different temperature.

Sample	Temp (°C)	Concentrations ppm (by wt.)	Concentrations μM	LPR R'_p (Ω cm^2)	LPR θ^a	LPR η(%)
4	60	0	0	2.38	-	-
		0.54	1.75	4.97	0.521	52.1
		1.49	4.84	6.50	0.634	63.4
		2.70	8.78	10.1	0.765	76.5
		5.42	17.6	17.1	0.861	86.1
		8.07	26.2	26.4	0.910	91.0
		10.8	35.2	30.9	0.923	92.3
		21.6	70.3	36.1	0.934	93.4
		54.2	176	37.8	0.937	93.7
5	50	0	0	1.89	-	-
		0.57	1.75	5.68	0.66.7	66.7
		1.57	4.84	6.77	0.721	72.1
		2.84	8.78	7.97	0.763	76.3
		5.70	17.6	9.74	0.806	80.6
		8.48	26.2	12.0	0.842	84.2
	60	0	0	2.38	-	-
		0.32	1.00	6.47	0.632	63.2
		0.57	1.75	7.68	0.690	69.0
		1.57	4.84	9.83	0.758	75.8
		2.84	8.78	12.4	0.808	80.8
		5.70	17.6	16.9	0.859	85.9
		8.48	26.2	39.0	0.939	93.9
		11.4	35.2	49.6	0.952	95.2
		22.8	70.3	54.1	0.956	95.6
		57.0	176	76.8	0.969	96.9
	70	0	0	9.29	-	-
		0.57	1.75	23.2	0.599	59.9
		1.57	4.84	29.0	0.680	68.0
		2.84	8.78	32.9	0.718	71.8
		5.70	17.6	42.0	0.779	77.9
		8.48	26.2	53.1	0.825	82.5
6	60	0	0	2.38	-	-
		0.59	1.75	4.23	0.438	43.8
		1.64	4.84	5.68	0.581	58.1
		2.98	8.78	7.96	0.701	70.1
		5.98	17.6	13.9	0.829	82.9
		8.90	26.2	16.0	0.851	85.1
		11.9	35.2	16.4	0.855	85.5
		23.9	70.3	17.1	0.861	86.1
		59.8	176	21.4	0.889	88.9

[a] Inhibition Efficiency, IE (i.e., η) = surface coverage θ.

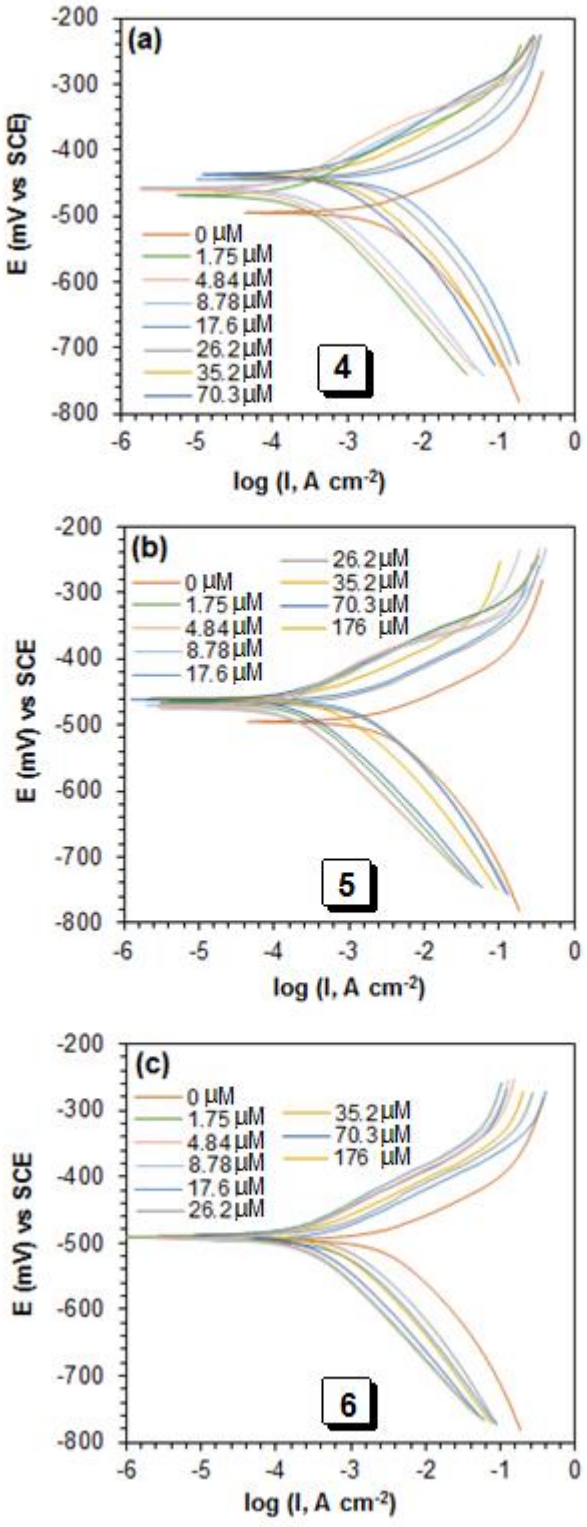

Figure 4. Potentiodynamic polarization curves at 60 ºC for mild steel in 1.0 M HCl solution containing different concentrations of **4**, **5** and **6**.

If the shifting of E_{corr} values is less than 85 mV, the inhibition can be considered either as cathodic or anodic type of inhibitor [33]. For the synthesized inhibitors in this study, the shifting was in between 20 to 65 mV towards positive direction which is not significant for the molecules to be classified as anodic type inhibitors. Fig. 4 showed that the inhibitor molecules **4-6** largely reduced the i_{corr} in the anodic than the cathodic branch. Consequently, inhibitor action is more pronounced in mitigating the iron dissolution at the anode than the cathodic reduction for hydrogen evolution. Therefore, the polymer molecules in this study are considered as mixed-type inhibitors under the influence of anodic control. The maximum decrease in current density (from 2465 to 61.6 $\mu A.cm^{-2}$) corresponds to η% of 97.5% was observed for sulfoxide **5** at 60 °C suggested it to be the best among the studied inhibitors (Table 3). The mechanism of the electrode reactions for the polymer compounds did not change since the slopes of β_c and β_a are not changed considerably; the inhibitors formed a barrier film on the metal surface and simply block the anodic and cathodic reaction sites. The polarizable electrons on sulfur and nitrogen through their interaction with the *d*-orbitals of iron or Fe^{2+} (*vide supra*) help adsorbing the polymer molecules on the anodic sites.

In Fig. 4, some of the anodic polarization curves display desorption potentials, which can be explained by the presence of current-increasing plateaus [34]. The presence of a desorption potential anticipates a pathway in which the polymer molecules initially imprison the anodic sites on the electrode and desorb at a higher potential that lead to enhance steel dissolution.

3.5. Impedance measurements

For better understanding the corrosion inhibition performance, the EIS experiments were carried out after 20 min immersion in the test solution. The recorded impedance data (Nyquist and Bode plots) of mild steel coupon/solutions in the presence or absence of different concentrations (1.75 to 176 µM) of inhibitors **4**, **5** and **6** were fitted by the Randles equivalent electrochemical circuit (the best fitted circuit) shown in Fig. 5. The simple circuit consists of a solution resistance (R_s), polarization resistance (R_p) and a constant phase element (CPE). The R_s was resulted by the potential drop between the mild steel coupon as a working electrode and the reference electrode, its value was calculated from intersecting the fitted semicircle with the real part (Z') axis at high frequency. While the R_p values were obtained from crossing the semicircle with Z' axis at low frequency, which were contributed by other resistances such as the charge transfer resistance and diffusion layer resistance at the surface of working electrode (mild steel coupon) [35]. The net polarization resistance (R'_p) at mild steel coupon was calculated using equation (5), and its values were used later to calculate the inhibition efficiencies based on the EIS using equation (3).

$$R'_p = R_p - R_s \quad (5)$$

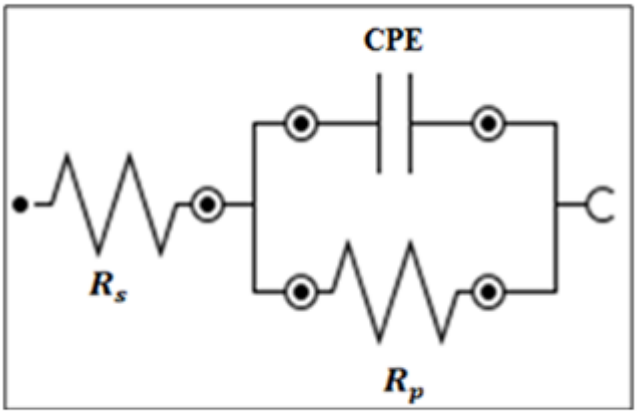

Figure 5. Randles electrochemical equivalent circuit diagram used for modeling metal/solution interface. R_s: Solution resistance, R_p: Polarization resistance, CPE: Constant phase element.

The CPE is used to express the non-ideal capacitance and non-ideal frequency response [36]. It is commonly used in the electrochemical circuit in order to attain better fitting. The double layer capacitance (C_{dl}) relates to the CPE by equation (6).

$$C_{dl} = \text{CPE}(\omega)^{n-1} \quad (6)$$

where ω is the angular frequency (radian) at the maximum imaginary part of the impedance and n is the surface heterogeneity.

Table 4. Impedance parameters for the corrosion of a mild steel sample in 1.0 M HCl solutions containing inhibitors **4, 5** and **6** at 60 °C.

Sample	Concentration		R_s (Ω cm^2)	R_p (Ω cm^2)	CPE^a (μF cm^{-2})	n	R'_p (Ωcm^2)	η(%)
	ppm (by wt.)	μM						
4	0	0	0.373	1.963	922	0.989	1.590	-
	0.54	1.75	0.560	3.950	635	0.909	3.390	53.1
	1.49	4.84	0.647	4.968	593	0.887	4.321	63.2
	2.70	8.78	0.628	7.452	393	0.831	6.824	76.7
	5.42	17.6	0.538	12.14	374	0.804	11.61	86.3
	8.07	26.2	0.838	17.57	292	0.853	16.74	90.5
	10.8	35.2	0.381	20.51	251	0.790	20.13	92.1
	21.6	70.3	0.317	24.78	115	0.753	24.46	93.5
	54.2	176	1.080	28.03	178	0.779	26.95	94.1
5	0	0	0.373	1.963	922	0.989	1.590	-
	0.32	1.00	0.568	4.948	446	0.916	4.380	63.7
	0.57	1.75	0.461	5.657	407	0.857	5.196	69.4

	1.57	4.84	0.393	7.046	490	0.860	6.653	76.1
	2.84	8.78	0.392	9.081	307	0.808	8.688	81.7
	5.70	17.6	0.336	11.86	323	0.713	11.52	86.2
	8.48	26.2	0.242	26.31	402	0.707	26.06	93.9
	11.4	35.2	0.757	36.89	400	0.715	36.14	95.6
	22.8	70.3	0.434	44.60	330	0.727	44.17	96.4
	57.0	176	0.389	53.39	358	0.709	53.00	97.0
6	0	0	0.373	1.963	922	0.989	1.590	-
	0.59	1.75	0.479	3.365	421	0.871	2.886	44.9
	1.64	4.84	0.530	4.343	356	0.787	3.813	58.3
	2.98	8.78	0.406	5.778	367	0.737	5.372	70.4
	5.98	17.6	0.392	10.46	339	0.781	10.06	84.2
	8.90	26.2	0.327	10.93	318	0.764	10.60	85
	11.9	35.2	0.392	11.51	303	0.825	11.12	85.7
	23.9	70.3	0.377	11.90	306	0.834	11.52	86.2
	59.8	176	0.631	15.22	259	0.857	14.59	89.1

[a]Double layer capacitance (C_{id}) and coating capacitance (C_c) are usually modelled with a constant phase element (CPE) in modeling an electrochemical phenomenon.

The EIS fitting results (Table 4) showed that the *n* values are lower than 1 which is attributed to the poor homogeneity of surface of the mild steel and decreasing with increase in the inhibitors concentration, which indicates increasing the heterogeneity of the surface. Table 4 summarizes the normalized EIS data for the corrosion of a mild steel sample in 1.0 M HCl solution containing different concentrations of inhibitors **4, 5** and **6** at 60 °C. It has been found that with the increase in the concentration of inhibitors, the R'_p were increased and the values of CPE were decreased as a result of increasing the thickness of the adsorbed inhibitor, this eventually leads to increase the inhibition efficiency of 97.0% in case of a concentration 176 µM of compound **5**. The lower *n* values at the higher concentrations of polymer molecules **4-6** suggested to increase in their adsorption on the metal surface, which leads to increase the heterogeneity of the metal surface.

The Nyquist and Bode plots are shown in Figs. 6 and 7 for different concentrations (1.75 to 176 µM) of inhibitors **4**, **5** and **6**. The inset in Fig. 6c shows the magnified corresponding Nyquist plots of blank (0 µM) and low concentrations (1.00 and 1.76 µM) of inhibitor **5**. In the Nyquist plots Fig. 6a, c and e, it was clear that increasing the diameter of the semicircle is related with the increase in the inhibitor concentrations, which depict an increase in the formed protective layer on the surface of the mild steel due to the adsorption of the inhibitor compounds. It was also noticed that the Nyquist plots don't appear with a perfect semicircle; therefore, the capacitance at the inhibitor solution-metal interface does not exhibit the properties of a real capacitor. The non-ideal or depressed semicircle in the Nyquist plots indicate the characteristic to the solution-solid electrode interface at a high to medium frequency, which is associated with the physical properties, such as surface roughness and inhomogeneity of the electrode [37].

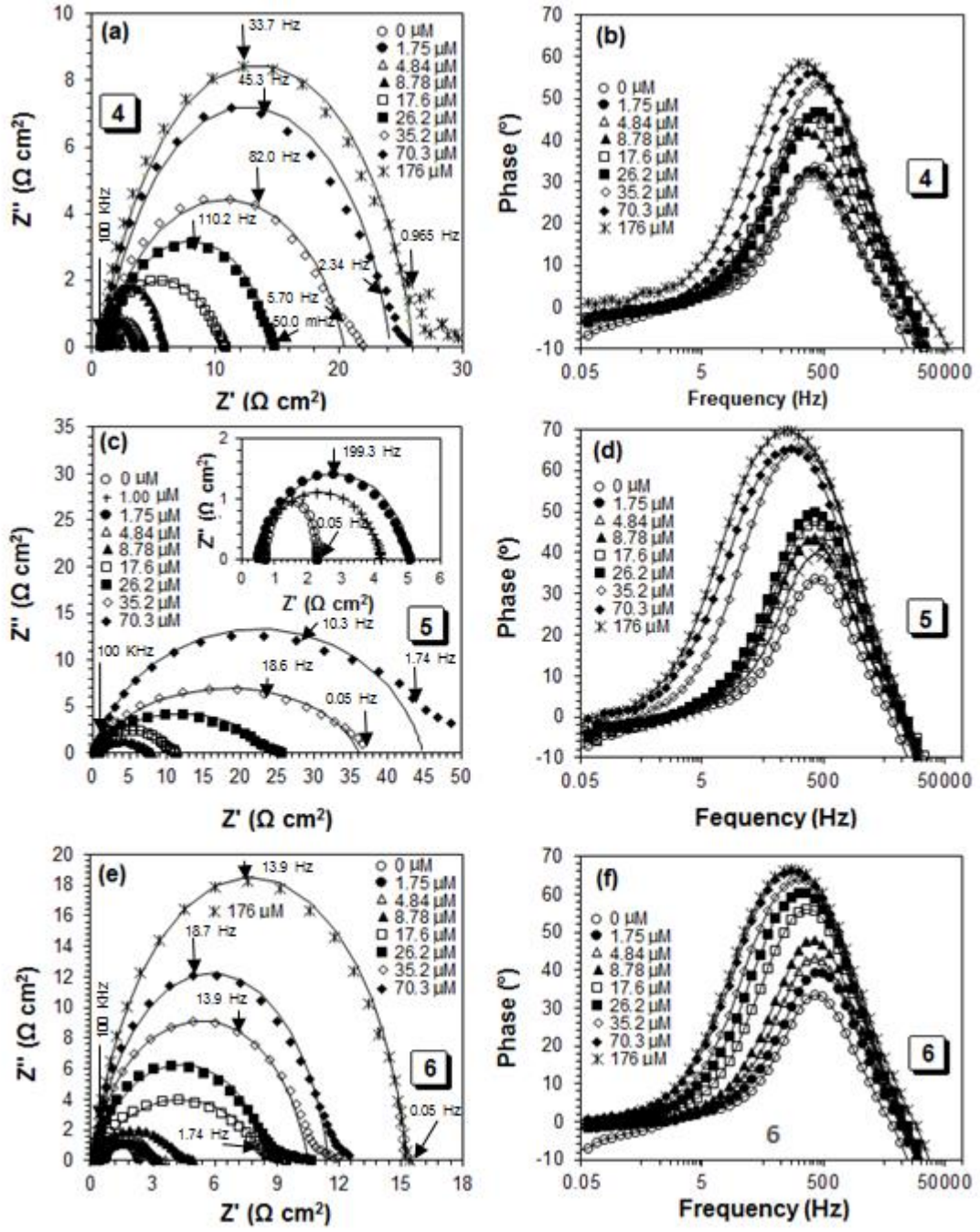

Figure 6. Nyquist diagram of (a) **4**, (c) **5** and (e) **6**, and Bode phase angle plots of (b) **4**, (d) **5** and (f) **6** of mild steel at 60 ºC in 1.0 M HCl containing various concentrations of inhibitors in 30 minutes' immersion time. Various symbols represent experimental data and solid lines in the Nyquist plot represent fitted data.

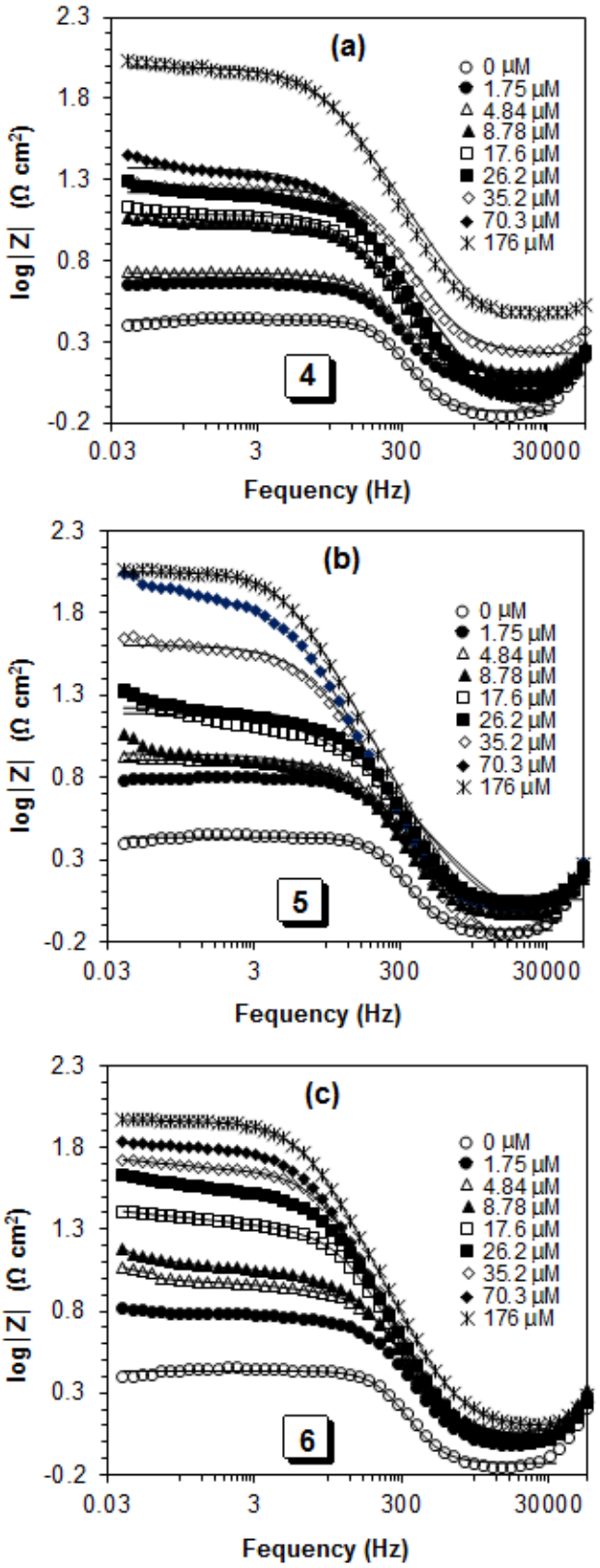

Figure 7. Bode impedance of (a) **4**, (b) **5** and (c) **6** of mild steel at 60 ºC in 1.0 M HCl containing various concentrations of inhibitors in 30 minutes' immersion time**.** Various symbols represent experimental data and solid lines in the Nyquist plot represent fitted data.

Bode phase angle plots (Fig. 6b, d and f) for compounds **4**, **5** and **6**, respectively showed an increase in the angle value at intermediate frequency with increasing the inhibitor concentrations, which demonstrates decreasing the capacitance at the surface of the mild steel electrode. It is attributed to decrease in the local dielectric constant as well as increasing the adsorbed amount of inhibitors on the coupon surface. Bode magnitude plots (Fig. 7) for compounds **4**, **5** and **6** imply an increase in the polarization resistance (R_p) with the increase in the inhibitor concentrations. However, these R_p can be obtained from intersection in the horizontal plateau region at low frequency with the y axis of log|Z|. Fig. 8(b-d) showed a comparison between the calculated inhibition efficiencies, whereas, the results obtained from EIS study confirmed the findings of the LPR, Tafel and gravimetric methods.

3.6. Adsorption isotherms

The inhibition efficiency (η) is equal to the surface coverage (θ) at lower concentrations where the polymer compounds form a monolayer on the metal surface. However, at higher concentrations the surface coverage transforms from monolayer to multilayers, and does not follow the linear relationship with increasing the concentrations. The Tafel extrapolations were used to determine the θ. The most common four adsorption isotherms (i.e. Freundlich, Langmuir, Frumkin and Temkin isotherms) describing the relationship between the surface coverage (θ) and the bulk low concentration of inhibitor (C) (Equations 7-10) [38] were tested using the linear least square method.

Freundluich: $\theta = K_{ads} C^{n}$ (7)

Langmuir: $\theta/(1-\theta) = K_{ads} C$ (8)

Frumkin: $K_{ads} C = \{\theta/(1-\theta)\} e^{-2\alpha\theta}$ (9)

Temkin: $K_{ads} C = e^{f\theta}$ (10)

Table 5. The values of the adsorption equilibrium constant[a], square of coefficient of correlation (R^2) and values of the constants in the adsorption isotherms of Temkin and free energy, enthalpy, entropy changes of the mild steel dissolution in the presence of inhibitor **5** in 1.0 M HCl.

Sample	Temp (°C)	Temkin (R^2, f)	K_{ads} (L mol^{-1})[b]	ΔG^o_{ads} (kJ mol^{-1})	ΔH^o_{ads} (kJ mol^{-1})	ΔS^o_{ads} (J mol^{-1} K^{-1})
5	50	0.9936, 15.9	5.96 x 10^{13}	-76.5		
	60	0.9985, 12.2	1.32 x 10^{12}	-72.4	-199	380
	70	0.9973, 12.9	3.83 x 10^{11}	-68.9		

[a]Used Tafel extrapolation plot

[b]K_{ads} obtained in L/mg was converted to L/mol.

The square correlation coefficients (R^2) and the values of the constants were determined from different adsorption isotherm models (Equations 7-10) for polymer sulfoxide **5** in 1.0 M HCl**.** As an evidence from the square correlation coefficients (R^2) obtained from different adsorption isotherm models, the synthesized polymer sulfoxide **5** in 1.0 M HCl was the best fitted by Temkin adsorption

isotherm (Table 5, Fig. 8). This indicates that the adsorption achieved through a complex mechanism by chemisorption and physisorption interactions.

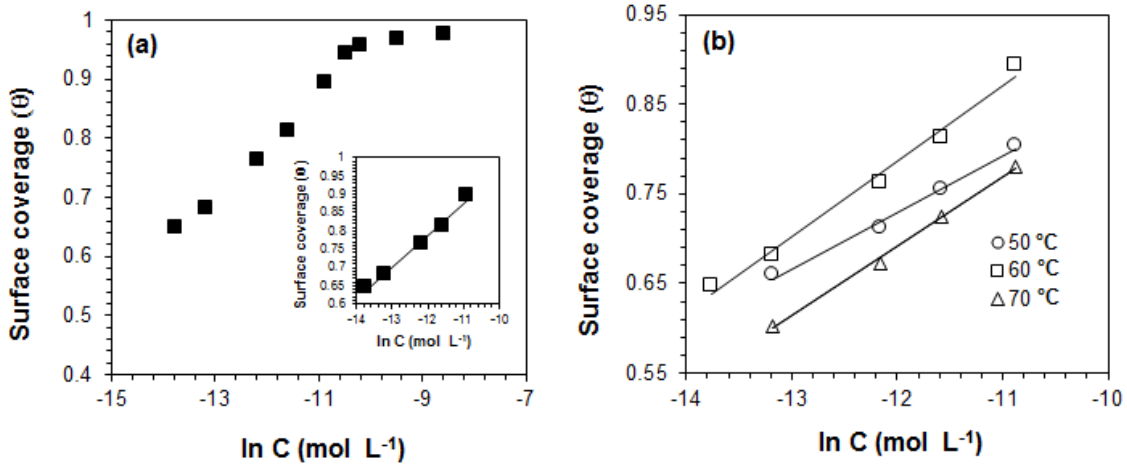

Fig. 8

Figure 8. Temkin adsorption isotherm for the adsorption of inhibitor **5** at (a) 60 °C and b) different temperatures (50-70 °C), on the surface of mild steel.

The adsorption mechanism was further investigated considering the thermodynamic parameters (adsorption equilibrium constant (K_{ads}), free energy (ΔG^{o}_{ads}), enthalpy (ΔH^{o}_{ads}) and entropy of adsorption ΔS^{o}_{ads}), which were calculated using equation (11), and presented in Table 5.

$$K_{ads} = \frac{1}{55.5} \exp\left(\frac{-\Delta G^{\circ}_{ads}}{RT}\right) \quad (11)$$

The negative values of ΔG^{o}_{ads} and ΔH^{o}_{ads} indicate the adsorption process is favorable and exothermic. Generally, the mechanism of adsorption can be classified as a physisorption or chemisorption or mixed mechanism based on the magnitude of ΔG^{o}_{ads} and ΔH^{o}_{ads}. When the absolute value of ΔG^{o}_{ads} is lower than 20 kJ mol^{-1} and the ΔH^{o}_{ads} is less negative than -40 kJ mol^{-1}, the adsorption process is described as physisorption. When the absolute value of ΔG^{o}_{ads} is higher than 40 kJ mol^{-1} and the ΔH^{o}_{ads} is more negative than -100 kJ mol^{-1}, the adsorption can be classified to be chemisorption. The adsorption process could be considered as mixed mechanism if the absolute value of ΔG^{o}_{ads} is higher than 20 kJ mol^{-1} but less than 40 kJ mol^{-1} [39-42]. Since the calculated values of ΔG^{o}_{ads} (-68.9 -76.5 kJ mol^{-1}) are more negative than -40 kJ mol^{-1} and ΔH^{o}_{ads} (-199 kJ mol^{-1}) is more negative than -100 kJ mol^{-1}, the adsorption of inhibitor **5** in this work is predominantly by chemisorption interaction. This means that the π and non-bonded electrons encourage the polymer molecules in various media undergoing a chemical interaction with the anodic sites *via* overlapping of nitrogen and sulfur lone pair of electrons with the low-lying vacant *d*-orbitals of iron [43,44]. The positive value of ΔS^{o}_{ads} (380 J mol^{-1} K^{-1}) for polymer **5** adsorption on mild steel is an indication of increasing the randomness on the solid surface/ inhibitor interface where the adsorbed inhibitor molecules displace the adsorbed water molecules on the surface of the mild steel (Fig. 9).

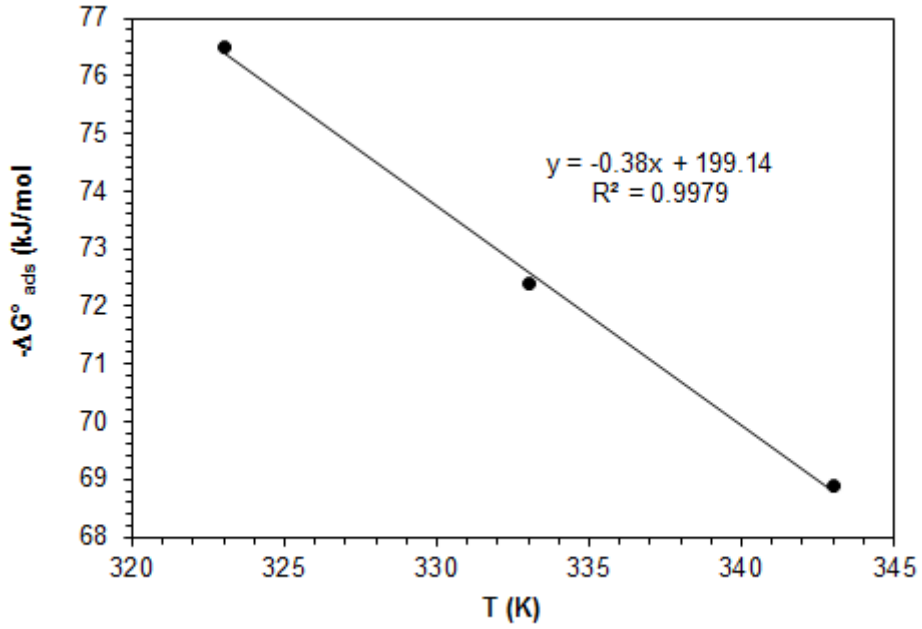

Figure 9. Variation of $-\Delta G^{o}_{ads}$ versus T on mild steel in 1.0 M HCl containing polymer **5.**

3.7. Surface tension

The surface tension and critical micelle concentration (CMC) value of all the polymer samples **4**, **5**, and **6** were determined by surface tensiometer in 1.0 M HCl solution at 60 ºC. Using the individual CMC values, the standard Gibbs free energy of micelle formation ***(***$\Delta G°_{mic}$***)*** was determined by the equation (12) [45].

$$\Delta G°_{mic} = RT \ln(C_{cmc}) \quad (12)$$

where R, T and C_{cmc} represent the gas constant, temperature and polymer concentration in mol L^{-1} at CMC.

The surface tension, CMC and $\Delta G°_{mic}$ values are reported in Table 6. The plot of the surface tension *vs* concentrations of the polymers is shown in Fig. 10a, while the percent inhibition efficiency *vs* concentration of the polymer profile is shown in Fig. 10b-d. The adsorption process was realized by measuring the surface tension of the studied polymers for micellaization. The surface tension as well as CMC value were found to be the lowest for polymer sulfide **4**, and progressively increase towards sulfoxide **5** and sulfone **6** motifs. The CMC values of polymer **4**, **5**, and **6** have been reported as 17.5, 19.1 and 20.9 µmol L^{-1}, respectively. For polymer sulfoxide **5**, at a concentration of 17.6 µM, the surface coverage (θ) of 87% confirmed that the polymer covered most of the surface before its concentration reached its CMC value of 19.5 µM in 1.0 M HCl (Fig. 10, Table 6). The CMC values (Fig. 10a, Table 6) and the surface coverage data (Fig. 10b-d) suggest that the polymer forms a monolayer and cover most of the surface before reaching their CMC, after that a multilayer can form due to the adsorption of micelles that could provide further protection to the metal surface [46]. The ΔG^{o}_{ads} values (≈ –72 kJ mol^{-1}, Table 5) obtained from Temkin adsorption isotherm are found to be

more negative than the corresponding ΔG^{o}_{mic} (≈ – 30 kJ mol^{-1}, Table 6), which further indicate that the adsorption of polymers onto the metal surface is preferred over micellization.

Table 6. Surface properties of compounds **4**, **5** and **6** in 1.0 M HCl solutions at 60 °C.

Compound	Surface tension (mN m^{-1})	C_{cmc} (μmol L^{-1})	C_{cmc} (ppm)	$\Delta G°_{mic}$ (kJ mol^{-1})
1M HCl	60.2	-	-	-
4	34.9	17.5	5.14	–30.3
5	39.2	19.1	6.22	–30.1
6	43.7	20.9	6.48	–29.8

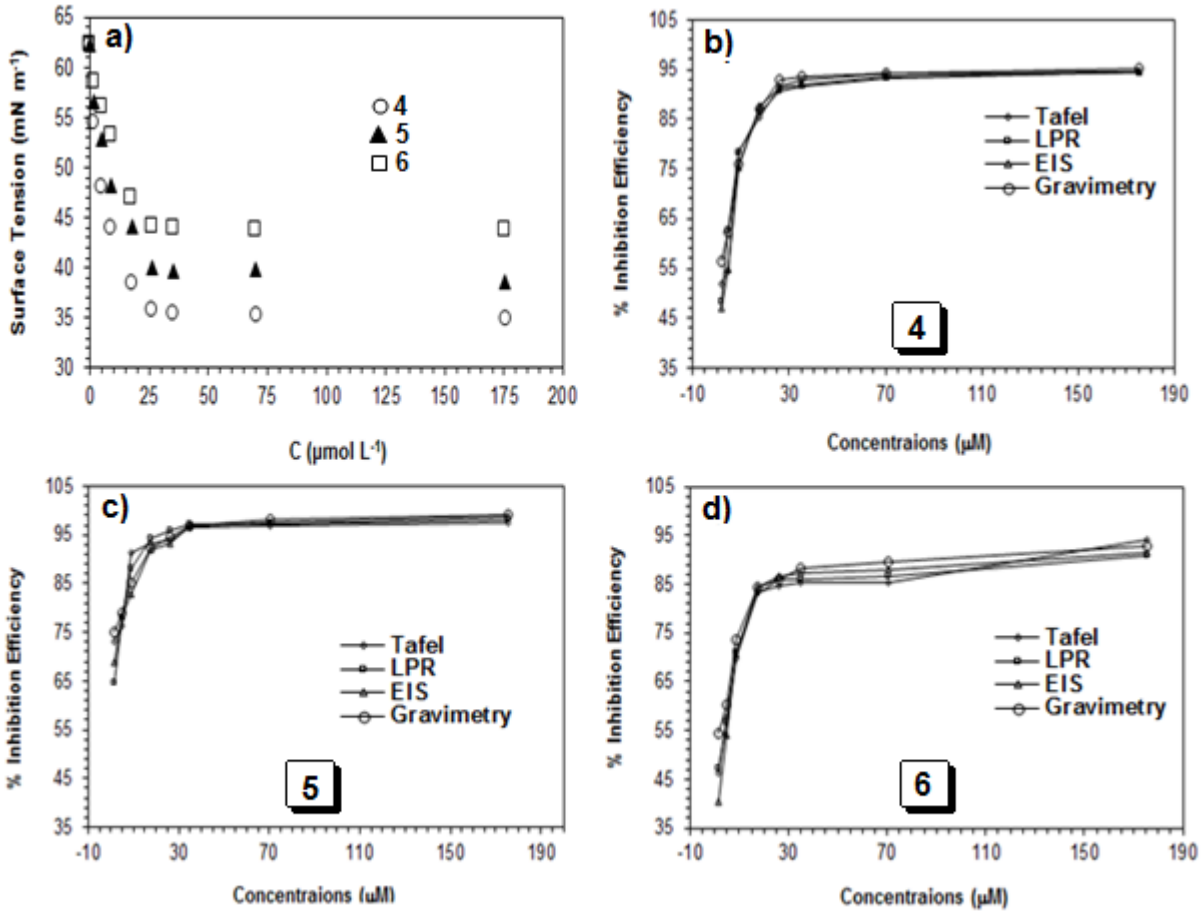

Figure 10. (a) Surface tension *versus* concentration, and (b) Inhibition efficiency *versus* concentrations profile of **4**, **5** and **6** in 1.0 M HCl solution at 60 ºC.

3.8. Surface analysis

The gravimetric and electrochemical test results showed the formation of protective film by the polymers. To further explore the inhibitive effects, the surface properties of the mild steel has been studied by XPS, SEM and EDX.

3.8.1. XPS analysis

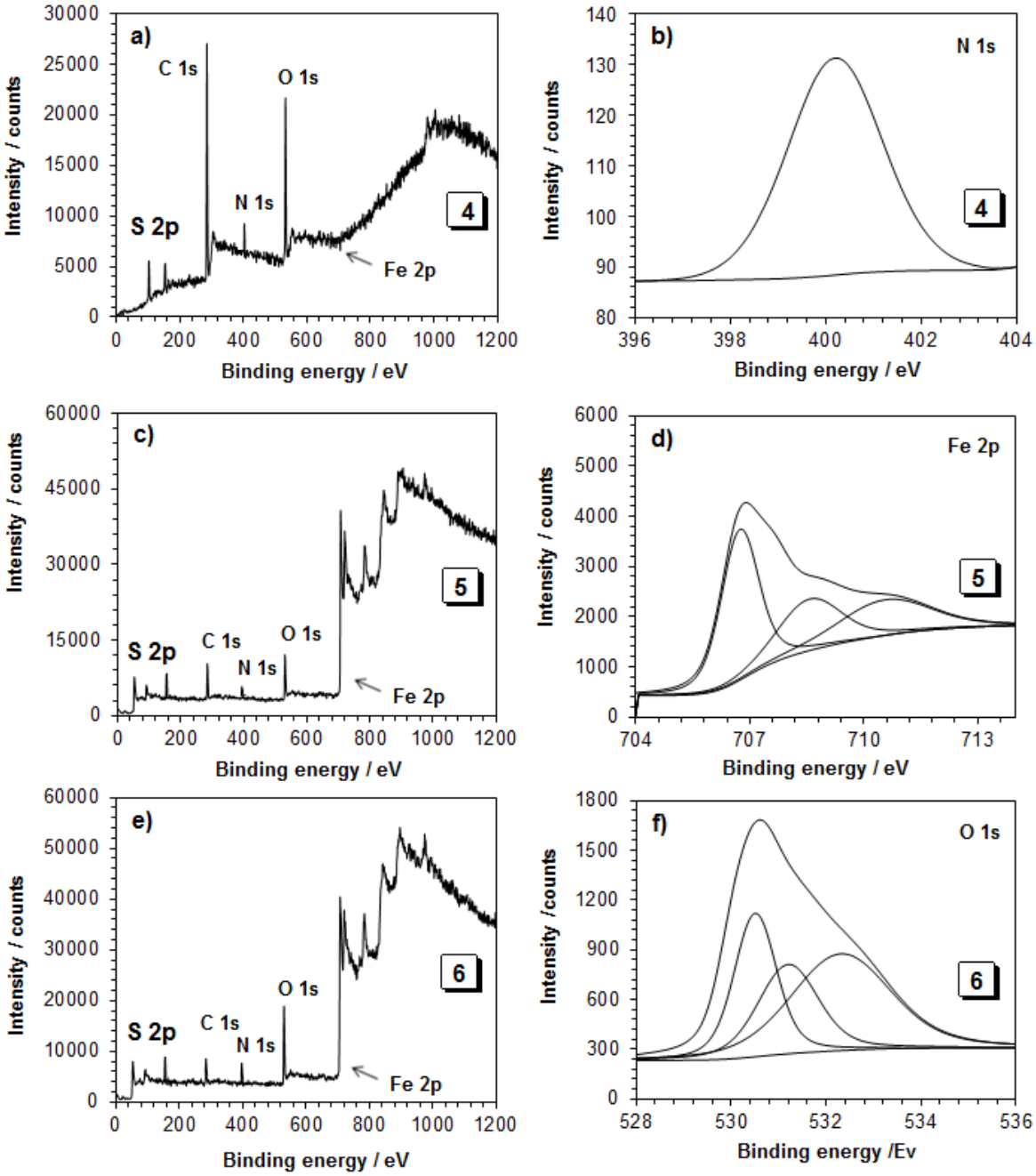

Figure 11. XPS survey spectrum of (a) **4**, (c) **5** and (e) **6**, and XPS deconvoluted profiles of (b) **4-** N 1s, (d) **5-** Fe 2p, and (f) **6-** O 1s in the presence of 176 μM inhibitors having an immersion time 6 h at 60 °C.

The polymeric thin films were prepared by immersing the mild steel coupons in 176 μM of polymer **5** in 1.0 M HCl solution for 6 h, and the intensity (counts) *versus* binding energy (eV) plots of the polymeric film covered mild steel were recorded by XPS, and are presented in Fig. 11a-f. The parameters obtained from XPS surface analysis are shown in Table 7. The wide scan spectra of polymeric film covered mild steel is shown in Fig. 11a, c, e. As shown in Fig. 11a, 11c and 11e, the signals of S 2p, N 1s, C 1s, O 1s ascertain the adsorption of polymer molecules onto the metal surface. It is worth mentioning that the sulfide and sulfoxide-type peaks usually appear near 162.2 and 168.2 eV, respectively [47].

Table 7. XPS scan composition of mild steel coupon in 1.0 M HCl containing **4, 5** and **6** at 60 °C

Peak	Approx. binding energy (eV)	Composition (atom %)		
		4	**5**	**6**
C 1s	285.3	34.9	30.7	32.2
C 1s	286.5	8.32	22.5	19.8
C 1s	288.4	13.1		
O 1s	530.1		25.9	13.1
O 1s	532.4	29.7	11.8	16.4
O 1s	533.3	10.5		12.2
N 1s	400.3	1.03	3.46	3.14
Fe 2p	707.3	1.26	1.98	1.45
Fe 2p	709.2	0.58	1.67	0.72
Fe 2p	712.6	1.02	2.20	1.07

Fig 11(b, d, f) presents the high resolution spectra of N 1s, Fe 2p and O 1s. The N 1s spectra revealed a peak near 400 eV, which indicates the presence of polymer onto the surface (Fig. 11b). The intensity signals appear at 713, 709 and 707 are attributed respectively to the presence of Fe^{3+} (2p), Fe^{2+} (2p) and Fe^{0} (2p) (Fig. 11d). The presence of O 1s peaks at 533.3, 531.8 and 530.1 shown in Fig 11f can be associated with the fact that all these studied polymers are of the type C=O, C-O and O^{2-} thereby implying the interaction between the polymer molecules and the oxide layer, which help forming a thin film onto the metal surface [48,49].

3.8.2. SEM- EDX analysis

The surface morphology of the polished, untreated and polymer treated mild steel surface were studied by SEM after the immersion of the metal surface in 1.0 M HCl for 6 h, and are presented in Fig. 12a-c. Fig. 12a shows the surface morphology of the polished mild steel sample, used as a reference. The uninhibited metal surface, shown in Fig. 12b, is drastically damaged, and appear to be intensely corroded, rough and porous after exposure to the acid (1.0 M HCl). However, in the presence

of polymer (176 μM), the surface morphology of the mild steel surface shown in Fig. 12c is remarkably improved having smooth surface compared to the untreated surface immersed in acid solution, due to the formation of protective layer by the constituents of polymer **5** onto the metal surface, and reduce the rate of corrosion of mild steel in 1.0 M HCl solution.

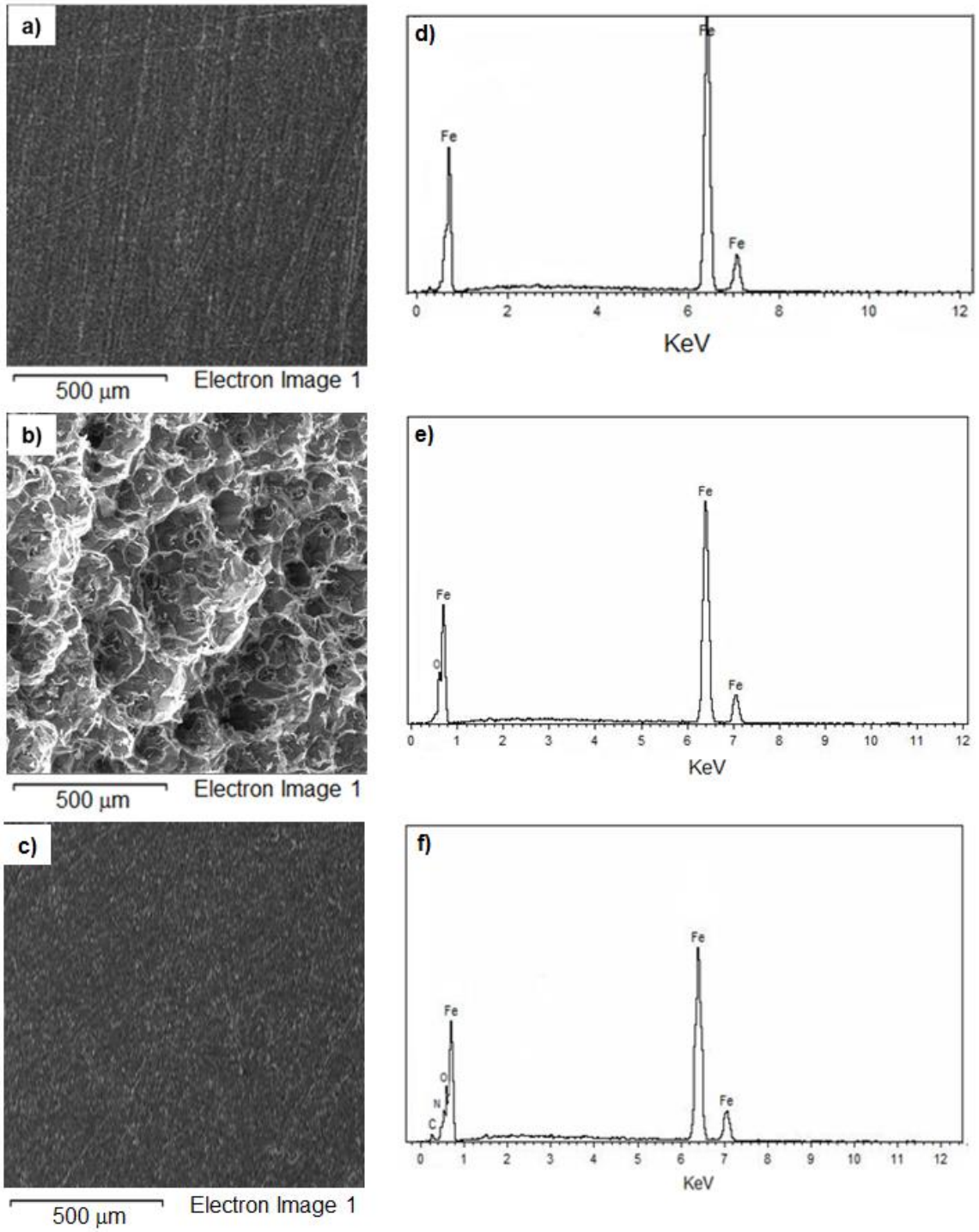

Figure 12. SEM and EDX of mild steel: a) untreated, b) treated with 1.0 M HCl, and c) treated with polymer **5** in 1.0 M HCl solution.

The EDX analysis was also performed to further confirm the adsorption of the polymer sulfoxide **5** onto the mild steel surface. The EDX analysis results of the polished, untreated and polymer treated mild steel surface are shown in Fig 12d-f. The strong iron signal is detected for the polished mild steel sample (Fig. 12d). For untreated mild steel specimen, the presence of iron and oxygen signals are attributed to the slow atmospheric oxidation, and form Fe_2O_3 oxide films (Fig. 12e). However, the EDX spectra of polymer treated sample (Fig. 12f), which showed the decrease in the intensity signal of iron along with additional signals of carbon, nitrogen and oxygen atoms confirmed that the studied polymer compounds are adsorbed onto the metallic surface, and implies the formation of protective film on the metal surface and shield the surface from further corrosion attack.

4. CONCLUSIONS

In the present study, the biogenic amino acid methionine residue in each repeating unit as a form of sulfide, sulfoxide or sulfone have been synthesized, characterized and investigated in detail for their feasibility as a corrosion inhibitor in acid media. The following conclusions have been drawn from this study:

1. The studied synthesized polymers act as a good corrosion inhibitor for mild steel corrosion in 1.0 M HCl.
2. The corrosion efficiency increases with increasing the concentration of the polymers. The maximum corrosion inhibition efficiency values of polymers **4-6** were found to be ~93, 97 and 85%, respectively at a concentration as low as 70.3 μM.
3. The inhibitor compounds studied in this report are considered as mixed-type inhibitors under the influence of anodic control.
4. The potentiodynamic polarization studies suggest that the inhibitor molecules are strongly adsorbed on the active sites of the metal, forming a protective film and suppress the metal dissolution.
5. The EIS study revealed that the synthesized compounds adsorbed onto the metal surfaces, which indicates that the inhibiting compounds form a protective layer and quarantine the metal surface from the corrosive environment. This observation is also supported by the increased values of R_p and decreased values of CPE with increasing the concentration of the inhibitor molecules.
6. The adsorptive behavior of the inhibitor molecules on the metal surface were fitted well with Temkin, Langmuir and Freundlich adsorption isotherm.
7. The ΔG^o_{ads} values revealed that the adsorption of the inhibitor molecules follow chemisorption interaction, and the ΔS^o_{ads} values suggested increasing the randomness on the solid surface/ inhibitor interface where the adsorbed inhibitor molecules displace the adsorbed water molecules on the surface of the mild steel.
8. The XPS, SEM-EDX supported the adsorption and the film forming ability of the studied inhibitor compounds on the mild steel surface.

ACKNOWLEDGEMENTS
The author gratefully acknowledges the Chemistry Department, King Fahd University of Petroleum & Minerals (KFUPM) for providing excellent research facilities, and the Deanship of Scientific Research (DSR), KFUPM, Saudi Arabia for financial assistance through the Internal Project # IN131047.

References

1. J. Mosa, N. C. Rosero-Navarro, M. Aparicio, *RSC Adv.*, 6 (2016) 39577.
2. C. Verma, L. O. Olasunkanmi, E. E. Ebenso, M. A. Quraishi, I. B. Obot, *J. Phys. Chem.*, 21 (2016) 11598.
3. A. O. James, N. Oforka, K. A. Olusegun, *Int. J. Electrochem. Sci.*, 2 (2007) 278.
4. S. A. Odoemelam, N. O. Eddy, *J. Surf. Sci. Technol.*, 24 (2008) 65.
5. P. Mourya, S. Banerjee, R. B. Rastogi, M. M. Singh, *Ind. Eng. Chem. Res.*, 52(36) (2013) 12733.
6. G. Trabanelli, V. Caraaiti, in: *Advances in corrosion science and technology*, vol. 1, Eds. M.G. Fontana, R.W. Staehle, Plenum Press, New York (1970).
7. M. A. Kiani, M. F. Mousavi, S. Ghasemi, M. Shamsipur, S. H. Kazemi, *Corros. Sci.*, 50 (2008) 1035.
8. M. A. Amin, K. F. Khaled, Q. Mohsen, H. A. Arida, *Corros. Sci.*, 52 (2010) 1684.
9. W. Revie, H. H. Uhlig, *Corrosion and corrosion control: An introduction to corrosion science and Engineering*, Wiley-Inter science, New York (2008).
10. Y. Tang, X. Yang, W. Yang, Y. Chen, R. Wan, *Corros. Sci.*, 52 (2010) 242.
11. P. J. Dunn, K. K. Hii, M. J. Krische, M. T. Williams (Eds.), *Sustainable catalysis: Challenges and practices for the pharmaceutical and fine chemical industries*, Wiley, Weinheim (2013).
12. R. A. Sheldon, *Green Chem.*, 16 (2014) 950.
13. H. Zhao, X. Zhang, L. Ji, H. Hud, Q. Li, *Corros. Sci.*, 83 (2014) 261.
14. D-Q. Zhang, Q-R. Cai, X-M. He, L-X. Gao, G. S. Kim, *Mater. Chem. Phys.*, 114 (2009) 612.
15. H. Ashassi-Sorkhabia, M. R. Majidib, K. Seyyedi, *Appl. Surf. Sci.*, 225 (2004) 176.
16. S. Zor, F. Kandemirli, M. Bingul, *Protection of metals and physical chemistry of surfaces*, Pleiades Publishing Ltd, Moscow (2009).
17. K. F. Khaled, *Corros. Sci.*, 52 (2010) 3225.
18. M. Mobin, S. Zehra, M. Parveen, *J. Mol. Liq.*, 216 (2016) 598.
19. G. Markevicius, S. Chaudhuri, C. Bajracharya, R. Rastogi, J. Xiao, C. Burnett, T. Q. Chastek, *Prog. Org. Coat.*, 75 (2012) 319.
20. S. Kumar, H. Vashisht, L. O. Olasunkanmi, I. Bahadur, H. Verma, M. Goyal, G. Singh, E. .E Ebenso, *Ind. Eng. Chem. Res.*, 56 (2017) 441.
21. R. Baskar, M. Gopiraman, D. Kesavan, K. Subramanian, S. Gopalakrishnan, *J. Mater. Eng. Perform.*, 24 (2015) 2847.
22. Y. Jianguo, W. Lin, V. Otieno-Alego, D. P. Schweinsberg, *Corros. Sci.*, 37 (1995) 975.
23. G. B. Butler, *Cyclopolymerization and cyclocopolymerization*, Marcel Dekker, New York (1992).
24. W. Jaeger, J. Bohrisch, A. Laschewsky, *Prog. Polym. Sci.*, 35 (2010) 511.
25. P. K. Singh, V. K. Singh, M. Singh, *E-Polymers*, 030 (2007) 1.
26. H. A. Al-Muallem, M. A. J. Mazumder, M. K. Estaitie, S. A. Ali, *Iran. Polym. J.*, 24 (2015) 541.
27. G. B. Butler, R. J. Angelo, *J. Am. Chem. Soc.*, 79 (1957) 3128.
28. G. Perdoncin, G. Scorranto, *J. Am. Chem. Soc.*, 99 (1977) 6983.
29. J. A. Davies, *Adv. Inorg. Chem. Radiochem.*, 24 (1981) 115.
30. M. Calligaris, O. Carugo, *Coord. Chem. Rev.*, 153 (1996) 83.
31. G. H. Lushington, A. B. Cowley, S. Silchenko, G. S. Lukat-Rodgers, K. R. Rodgers, D. R. Benson, *Inorg. Chem.*, 42 (2003) 7550.
32. Y. Niu, S. Feng, Y. Ding, R. Qu, D. Wang, J. J. Han, *Int. J. Quantum Chem.*, 110 (2010) 1982.

33. S. Z. Duan, Y. L. Tao, *Interface chemistry*, Higher education press, Beijing (1990).
34. F. Bentiss, M. Triasnel, M. Lagrenee, *Corros. Sci.*, 42 (2000) 127.
35. M. Erbil, *Chimica Acta Turci.* , 1 (1988) 59.
36. M. *Ö*zcan, E. Karadag, I. Dehri, *Colloids Surf A Physicochem Eng Asp.*, 316 (2008) 55.
37. R. *Yildiz*, T. *Doğan*, I. *Dehri, Corros. Sci.*, 85 (2014) 215.
38. P. C. Okafor, X. Liu, Y. G. Zheng, *Corros. Sci.*, 51 (2009) 761.
39. G. E. Badr, *Corros. Sci.*, 51 (2009) 2529.
40. R. M. El-Sherif, W. A. Badawy, *Int. J. Electrochem. Sci.*, 6 (2011) 6469.
41. T. Arslan, F. Kandemirli, E. E. Ebenso, I. Love, H. Alemu, *Corros. Sci.*, 5 (2009) 35.
42. L. Larabi, Y. Harek, M. Traisnel, A. Mansri, *J. Appl. Electrochem.*, 34 (2004) 833.
43. I. L. Rozenfeld, *Corrosion Inhibitors*, MacGraw-Hill, New York (1981).
44. L. Afia, R. Salghi, L. Bammou, E. Bazzi, B. Hammouti, L. Bazzi, A. Bouyanzer, *J. Saudi Chem. Soc.*, 18(1) (2014) 19.
45. H. J. Butt, K. Graf, M. Kappl, *Physics and Chemistry of Interfaces*, Wiley-VCH, Weinheim (2003).
46. K. Esumi, M. Ueno, *Structure performance relationships in surfactants*. Marcel Dekker Press, New York (2003).
47. G. W. Nelson, M. Perry, S. M. He, D. L. Zechel, J. H. Horton, *Colloids Surf. B*, 78 (2010) 61.
48. O. Olivares-Xometl, N. V. Likhanova, M. A. Domínguez-Aguilar, J. M. Hallen, L. S. Zamudio, E. Arce, *Appl. Surf. Sci.*, 252 (2006) 2139.
49. M. Tourabi, K. Nohair, M. Traisnel, C. Jama, F. Bentiss, *Corros. Sci.*, 75 (2013) 123.